Phosphofructokinase 1 Glycosylation Regulates Cell Growth and Metabolism

Wen Yi *et al.*

Science **337**, 975 (2012);
DOI: 10.1126/science.1222278

Science (print ISSN 0036-8075; online ISSN 1095-9203) is published weekly, except the last week in December, by the American Association for the Advancement of Science, 1200 New York Avenue NW, Washington, DC 20005.

displayed a subunit composition comparable to that of the wild-type complex (fig. S12B). Moreover, ectopic expression of wild-type mouse Su(z)12 efficiently rescued the deficiency of H3K27me3 levels in Su(z)12 null embryonic stem (ES) cells (*21*), but ectopic expression of comparable amounts of mouse Su(z)12 mutated at the same residues showed a much poorer rescue effect (Fig. 3E). These results collectively suggest that allosteric activation of PRC2 by neighboring nucleosomes is important for the establishment of H3K27me3 in vivo.

We propose that active genes are resistant to PRC2 activity not only because they carry active marks (such as H3K4me3, H3K36me2, and H3K36me3) that antagonize PRC2 activity (*20*, *22*) but also because the chromatin of actively transcribing genes is less compact, with a lower nucleosome density and a lower linker histone H1 content (*5*). Once active transcription has ceased upon transcription factor dissociation, either the chromatin-remodeling events or the incorporation of additional histones (including linker histones) would lead to higher nucleosome density, higher H1 content, and more compact chromatin structure, which in turn would convert these nucleosomes from their inert status to ideal substrates of PRC2. Thus, H3K27me3 could be established and lead to further repression of the target genes (fig. S13).

We studied the kinetics of chromatin compaction and H3K27me3 establishment in an ~1.8-kb region around the transcription start site of the *CYP26a1* gene (Fig. 4A) upon transcription cessation, because *CYP26a1* is an inducible gene regulated by retinoic acid (*23*) and a well-established Polycomb target repressed by H3K27me3 (*23*, *24*). Mouse ES cells were treated with retinoic acid for 36 hours to induce *CYP26a1* expression. Retinoic acid was then withdrawn to end the induction, and the cells were harvested at various time points after retinoic acid withdrawal (Fig. 4, B and C) to monitor the dynamic changes of the chromatin compaction status and H3K27me3 levels. The chromatin compaction status was determined by a nuclease accessibility assay (*25*). The tested regions displayed much more "open" structures upon induction, and they began to be less accessible at 2 to 4 hours and fully compacted at 8 hours after retinoic acid withdrawal (Fig. 4D). The establishment of H3K27me3 began at 8 hours and was complete at 36 hours after retinoic acid withdrawal (Fig. 4E). These results suggest that the local chromatin compaction precedes the establishment of H3K27me3, in agreement with our model.

The ability of PRC2 to distinguish active chromatin (open, marked by H3K4me3 and H3K36me2/3) from inactive chromatin (dense, marked by H3K27me3) provides a mechanistic solution for its ability to maintain (but not to initiate) the inactive states of target genes (fig. S13). Even so, compacted chromatin is not the sole determinant of PRC2 activity. Specific recruitment of PRC2 by Polycomb response elements (PREs) and DNA methylation–mediated antagonistic effect on PRC2 (*26*) are also important contributors for the overall landscape of PRC2-mediated H3K27 methylation profile.

References and Notes

1. R. Cao *et al.*, *Science* **298**, 1039 (2002); 10.1126/science.1076997.
2. B. Czermin *et al.*, *Cell* **111**, 185 (2002).
3. J. Müller *et al.*, *Cell* **111**, 197 (2002).
4. A. Kuzmichev, K. Nishioka, H. Erdjument-Bromage, P. Tempst, D. Reinberg, *Genes Dev.* **16**, 2893 (2002).
5. C. D. Allis, T. Jenuwein, D. Reinberg, *Epigenetics* (Cold Spring Harbor Laboratory Press, Cold Spring Harbor, NY, 2006).
6. Y. B. Schwartz, V. Pirrotta, *Curr. Opin. Cell Biol.* **20**, 266 (2008).
7. J. A. Simon, R. E. Kingston, *Nat. Rev. Mol. Cell Biol.* **10**, 697 (2009).
8. R. Cao, Y. Zhang, *Curr. Opin. Genet. Dev.* **14**, 155 (2004).
9. K. Plath *et al.*, *Science* **300**, 131 (2003); 10.1126/science.1084274.
10. R. Cao, Y. Zhang, *Mol. Cell* **15**, 57 (2004).
11. R. Margueron *et al.*, *Nature* **461**, 762 (2009).
12. K. H. Hansen *et al.*, *Nat. Cell Biol.* **10**, 1291 (2008).
13. C. Martin, R. Cao, Y. Zhang, *J. Biol. Chem.* **281**, 8365 (2006).
14. P. T. Lowary, J. Widom, *J. Mol. Biol.* **276**, 19 (1998).
15. D. E. Schones *et al.*, *Cell* **132**, 887 (2008).
16. A. Barski *et al.*, *Cell* **129**, 823 (2007).
17. L. Burdine, T. G. Gillette, H. J. Lin, T. Kodadek, *J. Am. Chem. Soc.* **126**, 11442 (2004).
18. A. Birve *et al.*, *Development* **128**, 3371 (2001).
19. C. S. Ketel *et al.*, *Mol. Cell. Biol.* **25**, 6857 (2005).
20. F. W. Schmitges *et al.*, *Mol. Cell* **42**, 330 (2011).
21. D. Pasini, A. P. Bracken, J. B. Hansen, M. Capillo, K. Helin, *Mol. Cell. Biol.* **27**, 3769 (2007).
22. W. Yuan *et al.*, *J. Biol. Chem.* **286**, 7983 (2011).
23. R. F. Gillespie, L. J. Gudas, *J. Mol. Biol.* **372**, 298 (2007).
24. L. A. Boyer *et al.*, *Nature* **441**, 349 (2006).
25. S. Rao, E. Procko, M. F. Shannon, *J. Immunol.* **167**, 4494 (2001).
26. H. Wu *et al.*, *Science* **329**, 444 (2010).

Acknowledgments: We appreciate K. Helin and Y. Shinkai for providing the Su(z)12 null and TT2 ES cells. This work was supported by the Chinese Ministry of Science and Technology (grants 2011CB812700 and 2011CB965300 to B.Z.; 2010CB944900 and 2011CB964800 to S.G.; and 2010CB835300 to J.C.), the Howard Hughes Medical Institute International Early Career Scientist Program (to B.Z.), and NSF Career award 0747475 (to X.J.Z.).

Supplementary Materials

www.sciencemag.org/cgi/content/full/337/6097/971/DC1
Materials and Methods
Supplementary Text
Figs. S1 to S16
References (*27*–*32*)

25 May 2012; accepted 12 July 2012
10.1126/science.1225237

Phosphofructokinase 1 Glycosylation Regulates Cell Growth and Metabolism

Wen Yi,[1,2] Peter M. Clark,[1,2] Daniel E. Mason,[3] Marie C. Keenan,[4] Collin Hill,[4] William A. Goddard III,[5] Eric C. Peters,[3] Edward M. Driggers,[4] Linda C. Hsieh-Wilson[1,2]*

Cancer cells must satisfy the metabolic demands of rapid cell growth within a continually changing microenvironment. We demonstrated that the dynamic posttranslational modification of proteins by O-linked β-*N*-acetylglucosamine (O-GlcNAcylation) is a key metabolic regulator of glucose metabolism. O-GlcNAcylation was induced at serine 529 of phosphofructokinase 1 (PFK1) in response to hypoxia. Glycosylation inhibited PFK1 activity and redirected glucose flux through the pentose phosphate pathway, thereby conferring a selective growth advantage on cancer cells. Blocking glycosylation of PFK1 at serine 529 reduced cancer cell proliferation in vitro and impaired tumor formation in vivo. These studies reveal a previously uncharacterized mechanism for the regulation of metabolic pathways in cancer and a possible target for therapeutic intervention.

Rapid physiological response is critical for the growth of tumors, which must satisfy the metabolic demands of increased cell proliferation in the face of a dynamically changing microenvironment. Cancer cells reprogram their cellular metabolism to generate molecules such as adenosine triphosphate (ATP), nucleotides, lipids, and reduced nicotinamide adenine dinucleotide phosphate (NADPH) to facilitate macromolecular synthesis and maintain redox homeostasis (*1*, *2*). Although mutations in tumor suppressors and oncogenic pathways contribute to these altered metabolic phenotypes (*1*–*3*), such changes are slower and relatively static. In contrast, posttranslational modifications such as protein phosphorylation allow cells to respond rapidly and reversibly to a wide range of signals.

The dynamic posttranslational glycosylation of proteins with O-linked β-*N*-acetylglucosamine

[1]Division of Chemistry and Chemical Engineering, California Institute of Technology, Pasadena, CA 91125, USA. [2]Howard Hughes Medical Institute, California Institute of Technology, Pasadena, CA 91125, USA. [3]Genomics Institute of the Novartis Research Foundation, San Diego, CA 92121, USA. [4]Agios Pharmaceuticals, 38 Sidney Street, Cambridge, MA 02139, USA. [5]Materials and Process Simulation Center, California Institute of Technology, Division of Chemistry and Chemical Engineering, 1200 East California Boulevard, Pasadena, CA 91125, USA.

*To whom correspondence should be addressed. E-mail: lhw@caltech.edu

(O-GlcNAcylation) serves as a nutrient sensor to couple metabolic status to the regulation of signaling pathways (*4*–*7*). O-GlcNAc transferase (OGT) catalyzes the transfer of *N*-acetylglucosamine from uridine diphospho-*N*-acetylglucosamine (UDP-GlcNAc) to serine or threonine residues of many intracellular proteins, including signaling proteins important for insulin resistance (*5*), oncogenes and tumor suppressors (*6*), and transcriptional coactivators that control gluconeogenesis (*7*). O-GlcNAc levels are increased in multiple tumor types, and OGT silencing inhibits breast tumor growth and prostate cancer metastasis (*6*, *8*, *9*).

O-GlcNAcylation can be rapidly induced (*10*) and is dynamically sensitive to changes in cellular UDP-GlcNAc concentrations (*4*). UDP-GlcNAc is biosynthesized from several key metabolites, including glucose, glutamine, acetyl–coenzyme A, uridine, and ATP (*11*, *12*). Consequently, UDP-GlcNAc may serve as a functional reporter of the status of various metabolic pathways. Indeed, UDP-GlcNAc and the hexosamine biosynthesis pathway couple growth factor–induced glutamine uptake to glucose metabolism through N-glycosylation of the interleukin-3 (IL-3) receptor (*11*). However, the fates of UDP-GlcNAc, particularly the functional consequences of dynamic O-GlcNAcylation in the regulation of cell metabolism, remain unknown.

To test whether O-GlcNAcylation directly couples nutrient sensing to cellular metabolism, we modulated O-GlcNAc concentrations and measured the effects on aerobic glycolysis. Global abundance of O-GlcNAc was increased by two- to fourfold in human lung cancer H1299 cells by overexpressing OGT or after pharmacological inhibition of β-*N*-acetylglucosaminidase (O-GlcNAcase or OGA), the glycosidase that removes O-GlcNAc, with *O*-(2-acetamido-2-deoxy-D-glucopyranosylidene)amino-*N*-phenylcarbamate (PUGNAc; Fig. 1A). Increasing the abundance

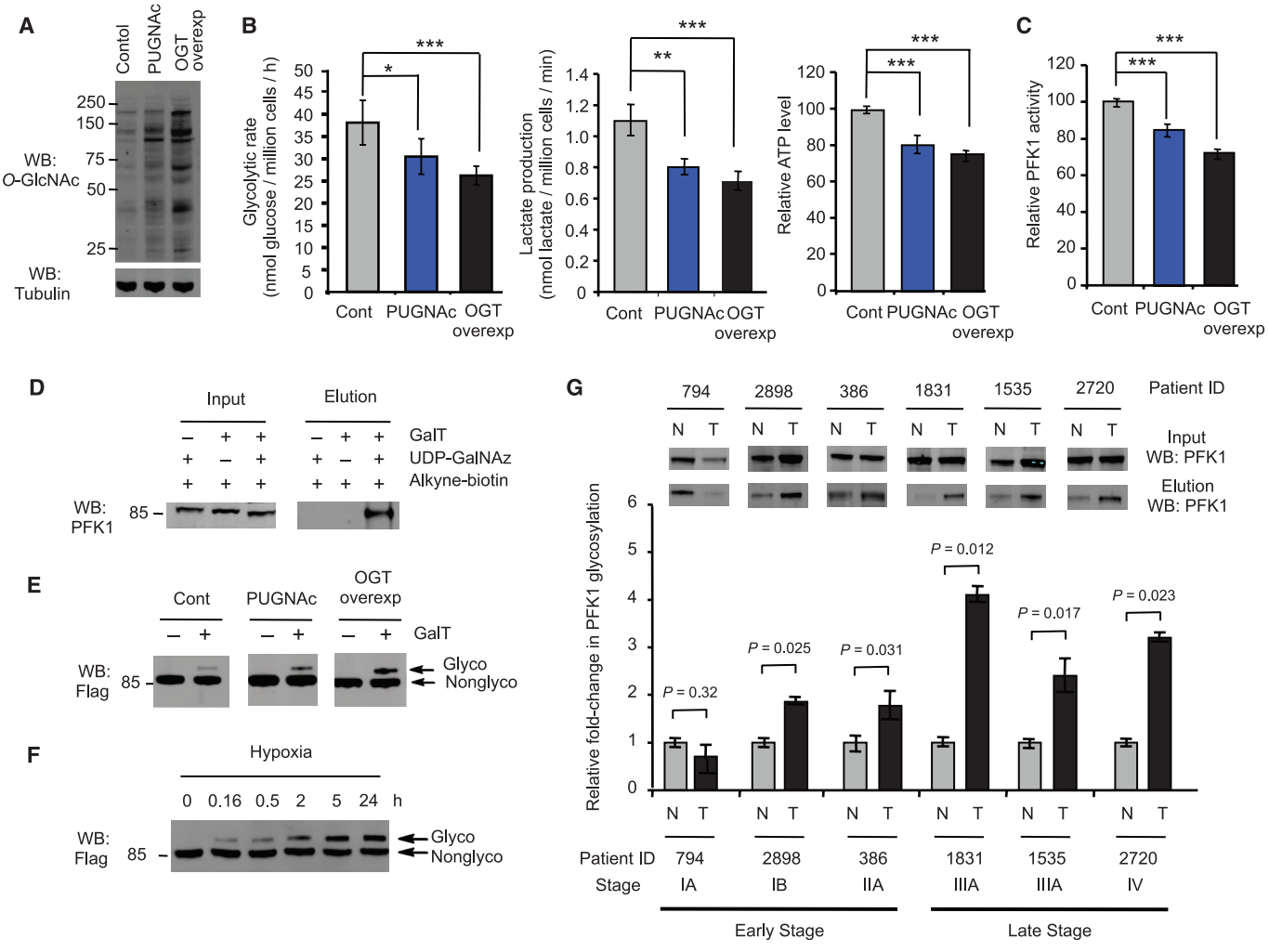

Fig. 1. Effects of O-GlcNAcylation on cellular metabolism and glycosylation of PFK1. (**A**) O-GlcNAcylation in H1299 cell lysates, as determined by immunoblotting for O-GlcNAc after treatment of cells with the OGA inhibitor PUGNAc or OGT overexpression. WB, Western blot. (**B**) Glycolytic rate, lactate production, and relative ATP levels in untreated (Cont), PUGNAc-treated, and OGT-overexpressing H1299 cells (n = 5 experiments). (**C**) PFK1 activity in untreated (Cont), PUGNAc-treated, and OGT-overexpressing 293T cells (n = 5 assays). (**D**) Detection of PFK1 glycosylation by protein immunoblotting after chemoenzymatic labeling of O-GlcNAc residues with UDP-GalNAz and the enzyme GalT, followed by reaction with an alkyne-biotin derivative, streptavidin precipitation, and elution of the biotinylated proteins. GalT or UDP-GalNAz was removed to confirm selective labeling of O-GlcNAc. (**E**) Detection of glycosylated PFK1 in 293T cells stably expressing Flag-tagged PFK1 by chemoenzymatic labeling with a 5-kD mass tag (*18*) and immunoblotting with a Flag antibody. Cells were untreated (Cont), PUGNAc-treated, or transfected to overexpress OGT. (**F**) Induction of PFK1 glycosylation under hypoxic conditions. H1299 cells stably expressing Flag-tagged PFK1 were cultured under 0.5% O_2 for the indicated times and rapidly lysed. Glycosylated PFK1 was detected after labeling with a 5-kD mass tag as above. (**G**) PFK1 glycosylation in human lung tumor (T) tissues compared to matched normal (N) tissues. O-GlcNAc–modified proteins from tissue lysates were biotinylated and detected as above. Relative PFK1 glycosylation was normalized using normal tissue for each patient. Error bars denote the standard error of the mean (SEM). Statistical analysis was performed by one-way analysis of variance (ANOVA) and Bonferroni comparison post-test in (B) and (C) and by Student's t test in (G) (*P < 0.05, **P < 0.01, ***P < 0.001).

of O-GlcNAc resulted in decreased rates of glucose metabolism relative to those of untreated cells under both normoxic and hypoxic conditions, as measured by the conversion of 5-^{3}H-glucose to ^3H_2O, which is catalyzed by enolase in the penultimate step of glycolysis (Fig. 1B and fig. S1). Enhancing O-GlcNAcylation also led to reduced lactate production and lowered cellular concentrations of ATP (Fig. 1B). Similar effects were observed in other cells, including invasive human lung cancer A549 cells and human embryonic kidney 293T cells (fig. S2). Because glycolytic flux is 5 to 15 times higher in cancer cells than flux through other central pathways in cancer cells (*13*), small alterations in glycolysis can result in substantial changes in the relative flow of branching pathways (*14*). To assess whether OGT-dependent glycosylation of protein substrates contributes to these effects, we stably depleted H1299 and 293T cells of OGT through the expression of short hairpin RNA (shRNA) (fig. S3). The inhibition of OGA in these OGT-deficient cells had no significant effect on glucose metabolism, lactate production, or ATP production (fig. S3).

Nearly all of the enzymes in the glycolytic pathway are putative substrates for OGT (*15*).

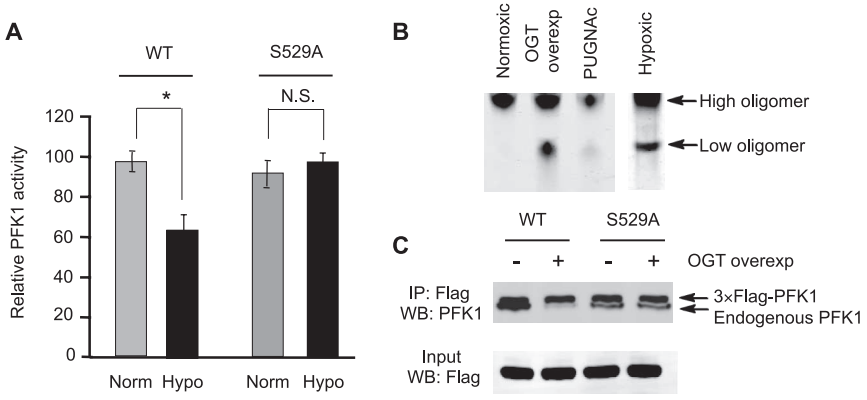

Fig. 2. Inhibition of PFK1 activity and oligomerization by glycosylation. (**A**) Relative activities of WT and S529A PFK1 (L isoform) purified from transfected 293T cells under normoxic or hypoxic conditions. Activities were measured in the presence of 100 μM F-2,6-BP and 3 mM ATP and were normalized with respect to the activity of WT PFK1 under normoxic conditions (n = 3 assays). (**B**) Oligomerization state of Flag-tagged PFK1 (L isoform) purified from 293T cells under normoxic or hypoxic conditions and from 293T cells overexpressing OGT or treated with PUGNAc under normoxic conditions. Complexes were resolved by nonreducing SDS–polyacrylamide gel electrophoresis (SDS-PAGE) and visualized by Coomassie blue staining. (**C**) Coimmunoprecipitation (IP) of endogenous PFK1 with Flag-tagged WT or S529A PFK1 (L isoform) after OGT overexpression. Complexes were immunoprecipitated with a Flag antibody conjugated to agarose beads and analyzed by reducing SDS-PAGE, followed by immunoblotting with a PFK1 antibody. Error bars denote SEM. Statistical analysis was performed by Student's t test (*P < 0.05).

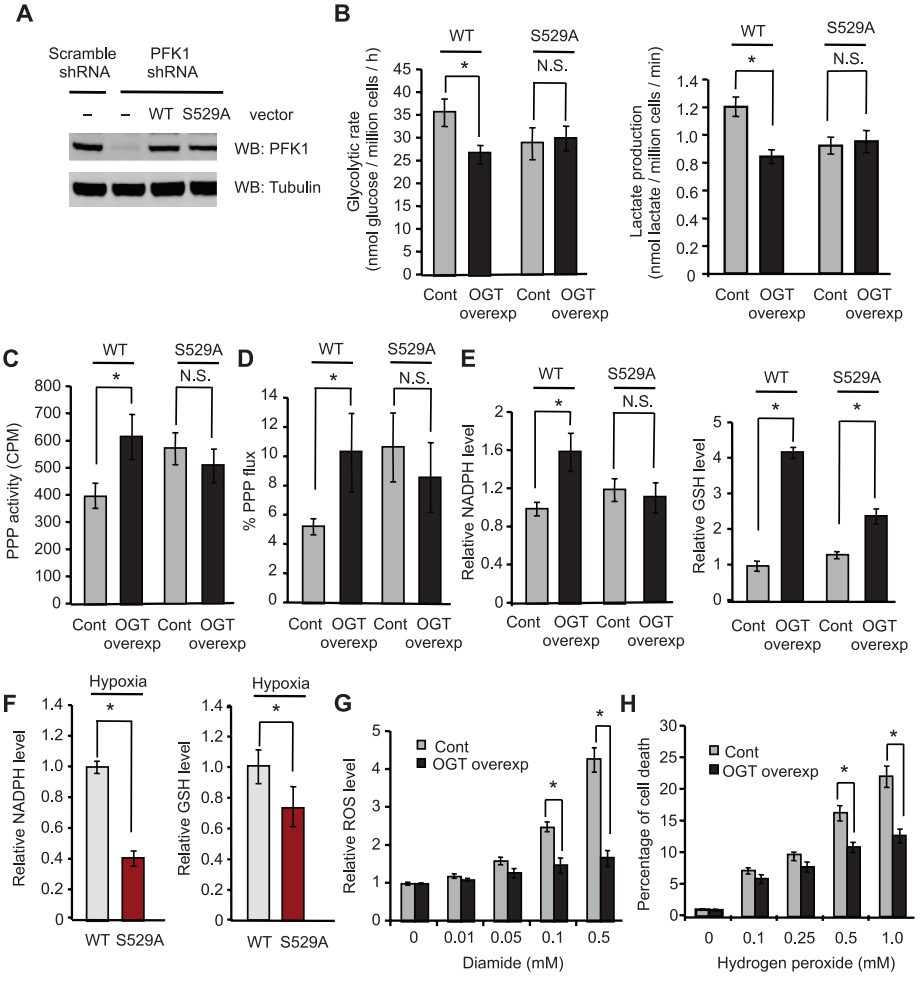

Fig. 3. PFK1 glycosylation at Ser^{529} regulates glycolysis, increases PPP flux, and protects cells from ROS-mediated cell death. (**A**) Immunoblotting of H1299 cells stably expressing shRNA and rescue constructs. Flag-PFK1 levels were comparable to endogenous PFK1 levels. (**B**) Glycolytic rate and lactate production of H1299 cells rescued with WT or S529A PFK1 in the absence (Cont) or presence of OGT overexpression (n = 4 experiments). (**C**) PPP activity in WT or S529A PFK1 rescue cells in the absence (Cont) or presence of OGT overexpression, as measured by the rate of $^{14}CO_2$ production from glucose via the PPP (n = 3 assays). (**D**) Percentage of central carbon flux from glucose to lactate flowing through the PPP in WT or S529A PFK1 rescue cells in the absence (Cont) or presence of OGT overexpression, as measured by reverse-phase triple-quadrupole liquid chromatography mass spectrometry. (**E**) NADPH and GSH levels in WT or S529A PFK1 rescue cells in the absence (Cont) or presence of OGT overexpression. NADPH and GSH concentrations are shown relative to WT PFK1 Cont and were assessed using a colorimetric assay and the thiol probe monochlorobimane, respectively (n = 4 experiments). (**F**) NADPH and GSH levels in WT or S529A PFK1 rescue cells under hypoxic conditions (n = 3 experiments). (**G**) Cellular ROS levels induced by varying concentrations of diamide in untreated H1299 cells (Cont) and H1299 cells overexpressing OGT, as measured by a fluorimetric assay. (**H**) Percentage of cell death induced by varying concentrations of hydrogen peroxide in untreated (Cont) and OGT-overexpressing H1299 cells, as measured by lactate dehydrogenase levels (n = 4 assays). Error bars denote SEM. Statistical analysis was performed by Student's t test (*P < 0.05) for all figures.

Thus, we modulated amounts of O-GlcNAc in 293T cells and assayed the activity of each enzyme in the pathway. Increased amounts of O-GlcNAc led to decreased activity of phosphofructokinase 1 (PFK1), a major regulatory enzyme that controls flux through glycolysis (*16*) (Fig. 1C). No change in the expression of PFK1 protein was observed (fig. S3). Enhancing the abundance of O-GlcNAc had little effect on other key regulatory points in the pathway, including hexokinase, phosphoglycerate kinase, and pyruvate kinase (fig. S4), nor did it affect other glycolytic enzymes.

To assess whether PFK1 is directly O-GlcNAcylated, we selectively labeled O-GlcNAc–modified proteins from 293T cell lysates with a non-natural azido sugar through exposure to an exogenous galactosyltransferase enzyme that specifically glycosylates terminal GlcNAc sugars (*15*, *17*) (fig. S5). Labeled proteins were then biotinylated through [3+2] azide-alkyne cycloaddition chemistry and isolated with streptavidin-agarose beads. Immunoblotting of the purified proteins with an antibody to PFK1 showed strong O-GlcNAcylation of PFK1 (Fig. 1D), which was further enhanced by overexpression of OGT (fig. S5). We also generated a stable cell line expressing Flag-tagged PFK1 and selectively labeled O-GlcNAc–modified proteins in the lysate with a 5-kD polyethylene glycol (PEG) mass tag to shift their molecular mass (*18*). Immunoblotting with an antibody to Flag enabled direct visualization of both the nonglycosylated and glycosylated species of Flag-PFK1 (Fig. 1E). The population of glycosylated PFK1 significantly increased upon OGT overexpression or OGA inhibition. Moreover, PFK1 glycosylation was induced under hypoxic conditions within minutes and accumulated in a time-dependent manner on 32.3 ± 3.8% of PFK1 (Fig. 1F and fig. S6). Glycosylation was also stimulated when cells were deprived of glucose (13.3 ± 2.2%; fig. S6), consistent with previous reports that O-GlcNAc levels and OGT expression are increased by nutrient deprivation and other forms of cell stress (*19*, *20*).

PFK1 was glycosylated in multiple cell lines from human solid tumors, including breast, prostate, liver, colon, and cervical cells, and glycosylation was greater in malignant than in non-tumorigenic breast and prostate cell lines (fig. S7). Glycosylation of PFK1 also occurred in human breast and lung tumor tissues and was significantly elevated by two- to fourfold in the majority of tumors relative to tumor-adjacent normal tissues from the same patient (Fig. 1G and fig. S8). Low-stage (stages I and II) lung adenocarcinoma tumors exhibited on average a 1.8-fold increase in PFK1 glycosylation as compared to that of the matched normal tissue, whereas high-stage (stages III and IV) lung adenocarcinomas showed an average 3.2-fold increase in glycosylation. PFK1 glycosylation was not induced in rapidly proliferating normal mouse T lymphocytes and human dermal fibroblast cells, as compared to their quiescent counterparts (fig. S9). Thus, PFK1 is modified with O-GlcNAc in cancer cells both in vitro and in vivo, and glycosylation is increased specifically under conditions associated with tumorigenesis and tumor growth.

To identify the glycosylation site(s) on PFK1, we transiently overexpressed Flag-tagged PFK1 and OGT in 293T cells. After immunoprecipitation and proteolytic digestion of PFK1, O-GlcNAcylated peptides were enriched by wheat germ agglutinin lectin affinity chromatography and subjected to electron transfer dissociation mass spectrometry analysis. We identified a single site of glycosylation at Ser^{529}, a highly conserved residue important for allosteric regulation of PFK1 by fructose-2,6-bisphosphate (F-2,6-BP) (*21*) (fig. S10). F-2,6-BP is the dominant activator of PFK1 at the high ATP concentrations (2 to 5 mM) found in cancer cells (*22*). The mutation of Ser^{529} to alanine (S529A) abolished the glycosylation of PFK1 in 293T cells, whereas alanine mutation of Thr^{527} had no effect (fig. S10).

Although no structure of human PFK1 is available, we used the *Saccharomyces cerevisiae* structure, which shares 82% sequence identity within the F-2,6-BP binding site, and the rabbit structure, which shares 97% sequence identity, to generate structural models of rabbit PFK1 complexed to F-2,6-BP and O-GlcNAcylated rabbit PFK1 (fig. S11; the root mean square deviation between the rabbit and yeast structures was only 1.70 Å). Ser^{529} formed a hydrogen bond with the 2-phosphate group of F-2,6-BP, and the O-GlcNAc moiety occupied the F-2,6-BP–binding pocket, indicating that O-GlcNAcylation might inhibit PFK1 activity by blocking binding of F-2,6-BP and disrupting PFK1 oligomerization.

To further examine the effects of O-GlcNAcylation on PFK1 activity, we expressed human Flag-tagged PFK1 (L, M, and P isoforms) in 293T cells in the presence or absence of hypoxic conditions, which enhance PFK1 glycosylation. Increasing O-GlcNAcylation of PFK1 by 25 to 33% because of hypoxia decreased the activity of all three isoforms by 21 to 36%, with the L and P isoforms being most sensitive to glycosylation (Fig. 2A and fig. S12).We then focused on the L isoform of PFK1, whose expression is enhanced in multiple cancer cells (*23*). Hypoxia produced no significant change in PFK1 activity

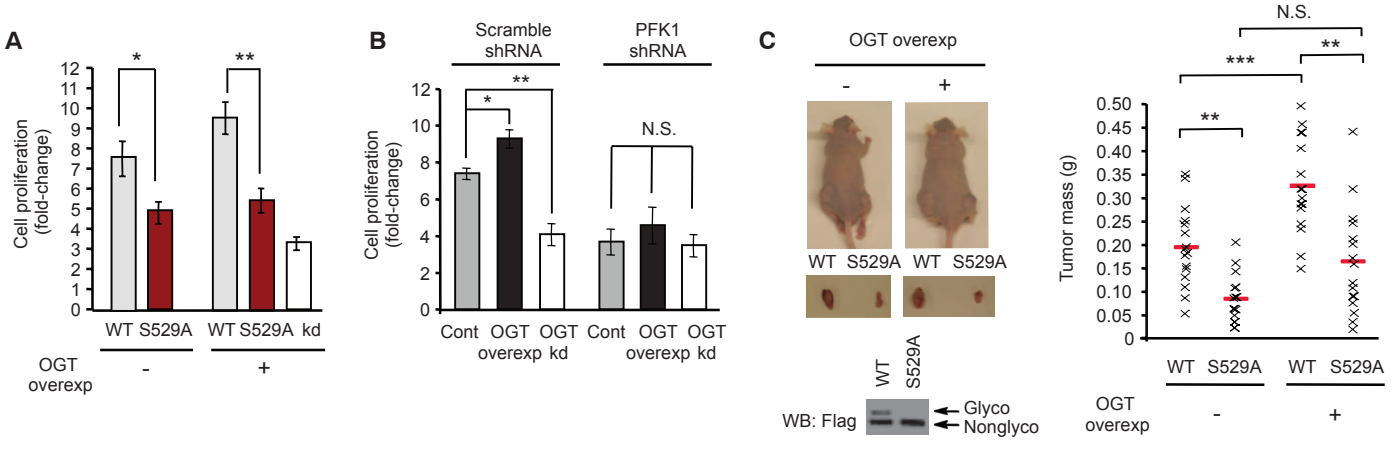

Fig. 4. PFK1 glycosylation contributes to cell proliferation and tumor growth. (**A**) Cell proliferation rates under hypoxic conditions of WT and S529A PFK1 H1299 rescue cells with and without OGT overexpression, as measured by the amount of cellular ATP (n = 3 experiments). (**B**) Cell proliferation rates under hypoxic conditions of H1299 cells infected with lentiviruses containing scrambled or PFK1 shRNA constructs after no treatment (Cont), OGT knockdown, or OGT overexpression (n = 3 experiments). (**C**) Tumor formation in nude mice injected with WT or S529A PFK1 H1299 rescue cells with and without OGT overexpression. (Left, top) Dissected tumors after 7 weeks of growth in mice injected with WT cells on the left flank and S529A cells on the right flank. (Left, bottom) PFK1 glycosylation in tumor lysates originating from WT or S529A H1299 rescue cells after labeling with a 5-kD mass tag and immunoblotting with Flag antibody. (Right) Masses of the dissected tumors. Each x represents the mass from one mouse; the horizontal red line indicates the mean tumor mass. Error bars denote SEM. Statistical analysis was performed by one-way ANOVA and Bonferroni comparison post-test in (B) and (C) and by Student's t test in (A) (*P < 0.05, **P < 0.01, ***P < 0.001; N.S., not significant).

when Ser^{529} was mutated to alanine (Fig. 2A). Similar effects on PFK1 activity were observed when O-GlcNAcylation was increased by means of other cellular treatments (fig. S13). Furthermore, glycosylation inhibited PFK1 activity across a wide ATP concentration range in the presence and absence of F-2,6-BP (fig. S14). Consistent with the importance of Ser^{529} in recognition of the allosteric activator, the activity of S529A PFK1 was impaired at lower F-2,6-BP concentrations (fig. S15). Therefore, we examined the effects of glycosylation in the presence of endogenous F-2,6-BP concentrations in 293T cells or 8.5 μM F-2,6-BP, which is within the physiological range for cancer cells (*24*). In both cases, the activity of wild-type (WT) PFK1 was significantly lower than that of S529A PFK1 when glycosylation was induced by hypoxia (fig. S16). Glycosylation thus exerts a strong inhibitory effect on PFK1 activity, and the mutation of Ser^{529} to Ala rescues the inhibitory effect. These results indicate that O-GlcNAcylation of PFK1 at Ser^{529} provides a mechanism to overcome the allosteric regulation of PFK1 by ATP and F-2,6-BP.

F-2,6-BP slows the dissociation of complexes of PFK1 and promotes the association of PFK1 into tetramers and higher oligomers with enhanced catalytic activity (*16*). We expressed Flag-tagged PFK1 in 293T cells under normoxic or hypoxic conditions. After hypoxia treatment, a fraction of PFK1 exhibited faster mobility during native gel electrophoresis (Fig. 2B). A similar shift in mobility was observed when PFK1 glycosylation levels were increased by OGT overexpression or OGA inhibition and when PFK1 was heat-denatured (fig. S17), suggesting that this complex represents a lower oligomeric state of PFK1. We also examined the association of Flag-tagged PFK1 with endogenous PFK1 by coimmunoprecipitation. Overexpression of OGT impaired the coimmunoprecipitation of PFK1 subunits, and this effect was blocked by alanine mutation of Ser^{529} (Fig. 2C). Thus, O-GlcNAcylation not only inhibits the activity of PFK1 but also appears to perturb the equilibrium between different oligomeric forms.

To test the effects of PFK1 glycosylation on cellular metabolism, we depleted endogenous PFK1 and stably expressed Flag-tagged WT or S529A PFK1 in H1299 cells (henceforth referred to as WT PFK1 or S529A PFK1 rescue cells; Fig. 3A). Upon OGT overexpression, cells expressing WT PFK1 exhibited reduced glycolysis and lactate production relative to control cells (Fig. 3B). No change in glycolytic rate or lactate production was observed in cells expressing S529A PFK1 upon OGT overexpression.

Suppressing glycolysis can redirect metabolic flux down the oxidative pentose phosphate pathway (PPP) (*25*, *26*), providing cells with pentose sugars for nucleotide and nucleic acid biosynthesis, as well as NADPH to combat oxidative stress (*25*–*27*). We observed both increased total and proportional flux through the oxidative PPP pathway, as measured by the amount of released $^{14}CO_2$ from [1-^{14}C]-glucose, and by relative accumulation of singly versus doubly [^{13}C]-labeled lactate from a [1,2-^{13}C]-glucose feed, when O-GlcNAcylation was enhanced in WT PFK1 rescue cells (Fig. 3, C and D). In contrast, PPP flux remained unaffected in S529A PFK1 rescue cells; however, it was increased as compared to that of untreated WT PFK1 rescue cells, possibly because of inhibitory effects of the S529A mutation on PFK1 activity (fig. S15).

PPP flux generates NADPH, which maintains a pool of reduced glutathione (GSH) and combats reactive oxygen species (ROS)–mediated cell death (*24*, *28*). Consistent with increased PPP flux, enhancing abundance of O-GlcNAc by OGT overexpression in WT PFK1 rescue cells led to 1.6-fold and 4-fold increases in amounts of NADPH and GSH, respectively (Fig. 3E). Blocking glycosylation of PFK1 at Ser^{529} prevented the increase in NADPH and partially prevented the increase in GSH. Amounts of NADPH and GSH were also increased under hypoxic conditions in WT PFK1 rescue cells as compared to those in S529A PFK1 rescue cells (Fig. 3F). Furthermore, untargeted metabolite profiling by high-resolution flow-injection mass spectrometry (*29*) revealed enhanced steady-state concentrations of GSH, amino acids, and nucleotide precursors in WT PFK1 rescue cells relative to those in S529A PFK1 rescue cells (table S1). We measured the sensitivity of H1299 cells to ROS-mediated cell death upon overexpression of OGT. Enhancing O-GlcNAcylation prevented the increase in ROS levels induced by diamide (Fig. 3G) and protected the cells from hydrogen peroxide–mediated cell death (Fig. 3H). Thus, increases in PPP flux induced by PFK1 glycosylation might help promote cancer cell survival.

Cells expressing the S529A mutant proliferated more slowly than cells expressing WT PFK1 under hypoxic conditions, which is consistent with reduced flux through the PPP (Fig. 4A). The proliferation rate of WT PFK1-expressing cells was enhanced further upon OGT overexpression, whereas that of S529A PFK1-expressing cells was unchanged. OGT overexpression increased, whereas OGT depletion decreased, cell proliferation under hypoxic conditions (Fig. 4B). Depletion of PFK1 abolished these effects, indicating that O-GlcNAcylation stimulates cell proliferation through a PFK1-dependent mechanism (although decreasing PFK1 expression may blunt the differences in cell growth).

We injected immunocompromised mice (*nu*/*nu*) with WT PFK1 or S529A PFK1 rescue cells in the presence or absence of OGT overexpression (fig. S18) and assayed for tumor formation. Mice injected with S529A PFK1 rescue cells showed decreased tumor mass as compared to mice injected with WT PFK1 rescue cells (Fig. 4C). Moreover, overexpression of OGT in WT PFK1 rescue cells enhanced tumor growth but had no significant effect on S529A PFK1 rescue cells. Protein immunoblot analysis confirmed that the Flag-tagged WT or S529A PFK1 proteins were retained in the tumors and that WT PFK1 was O-GlcNAcylated (Fig. 4C). Under these conditions, glycosylation of PFK1 at Ser^{529} provides a critical growth advantage to tumor cells in vivo.

We demonstrated that O-GlcNAc glycosylation directly regulates glycolysis and reroutes metabolic flux through pathways critical for cancer cell proliferation and survival. O-GlcNAc can simultaneously sense and redirect flow through essential metabolic pathways, specifically through the modulation of PFK1 activity, adding a previously unrecognized mode of regulation to this glycolytic enzyme. Furthermore, because UDP-GlcNAc represents a key point of pathway integration and enables the cell to monitor the balance between glucose and glutamine uptake (*11*, *12*), O-GlcNAcylation of PFK1 may provide an important mechanism to link the availability of both carbon and nitrogen sources for the cell to the production of metabolites necessary for sustaining rapid tumor growth.

Hypoxia also activates PFK1 glycosylation, thereby redirecting a larger fraction of the glucose flux through the PPP and increasing biosynthetic precursors, as well as reducing power from increased NADPH and GSH, to impart a growth advantage to cancer cells. Our results suggest that dynamic physiological inhibition of PFK1 may be a major regulatory point for central carbon flow. Blocking PFK1 glycosylation to enhance its activity and reset cellular metabolism toward normal cell growth could therefore provide a new strategy to combat cancer.

References and Notes

1. M. G. Vander Heiden, L. C. Cantley, C. B. Thompson, *Science* **324**, 1029 (2009).
2. R. A. Cairns, I. S. Harris, T. W. Mak, *Nat. Rev. Cancer* **11**, 85 (2011).
3. A. J. Levine, A. M. Puzio-Kuter, *Science* **330**, 1340 (2010).
4. G. W. Hart, M. P. Housley, C. Slawson, *Nature* **446**, 1017 (2007).
5. X. Yang *et al.*, *Nature* **451**, 964 (2008).
6. C. Slawson, G. W. Hart, *Nat. Rev. Cancer* **11**, 678 (2011).
7. R. Dentin, S. Hedrick, J. Xie, J. Yates 3rd, M. Montminy, *Science* **319**, 1402 (2008).
8. S. A. Caldwell *et al.*, *Oncogene* **29**, 2831 (2010).
9. T. P. Lynch *et al.*, *J. Biol. Chem.* **287**, 11070 (2012).
10. J. E. Rexach *et al.*, *Nat. Chem. Biol.* **8**, 253 (2012).
11. K. E. Wellen *et al.*, *Genes Dev.* **24**, 2784 (2010).
12. H. N. Moseley, A. N. Lane, A. C. Belshoff, R. M. Higashi, T. W. Fan, *BMC Biol.* **9**, 37 (2011).
13. Y. Sidorenko, A. Wahl, M. Dauner, Y. Genzel, U. Reichl, *Biotechnol. Prog.* **24**, 311 (2008).
14. R. Possemato *et al.*, *Nature* **476**, 346 (2011).
15. P. M. Clark *et al.*, *J. Am. Chem. Soc.* **130**, 11576 (2008).
16. M. Sola-Penna, D. Da Silva, W. S. Coelho, M. M. Marinho-Carvalho, P. Zancan, *IUBMB Life* **62**, 791 (2010).
17. B. Ramakrishnan, P. K. Qasba, *J. Biol. Chem.* **277**, 20833 (2002).
18. J. E. Rexach *et al.*, *Nat. Chem. Biol.* **6**, 645 (2010).
19. N. E. Zachara *et al.*, *J. Biol. Chem.* **279**, 30133 (2004).
20. R. P. Taylor *et al.*, *J. Biol. Chem.* **283**, 6050 (2008).
21. C. Ferreras, E. D. Hernández, O. H. Martínez-Costa, J. J. Aragón, *J. Biol. Chem.* **284**, 9124 (2009).
22. X. Lu *et al.*, *Clin. Cancer Res.* **6**, 271 (2000).

23. A. Yalcin, S. Telang, B. Clem, J. Chesney, *Exp. Mol. Pathol.* **86**, 174 (2009).
24. K. Bensaad *et al.*, *Cell* **126**, 107 (2006).
25. A. Herrero-Mendez *et al.*, *Nat. Cell Biol.* **11**, 747 (2009).
26. D. Anastasiou *et al.*, *Science* **334**, 1278 (2011).
27. X. Tong, F. Zhao, C. B. Thompson, *Curr. Opin. Genet. Dev.* **19**, 32 (2009).
28. P. P. Pandolfi *et al.*, *EMBO J.* **14**, 5209 (1995).
29. T. Fuhrer, D. Heer, B. Begemann, N. Zamboni, *Anal. Chem.* **83**, 7074 (2011).

Acknowledgments: We thank P. Qasba for the Y289L GalT construct, R. Abrol for computational modeling advice, R. Diamond for cell cycle analysis, and L. Cantley and M. Vander Heiden for useful discussions. This work was supported by the National Institutes of Health (grant R01 GM084724 to L.C.H-W), the Department of Defense Breast Cancer Research Program (grant W81XWH-10-1-0988 to W.Y), and a Tobacco-Related Disease Research Program Postdoctoral Fellowship (19FT-0078 to W.Y). We also thank Agios Pharmaceuticals for financial support in providing patient tumor and matched tissue samples.

Supplementary Materials
www.sciencemag.org/cgi/content/full/337/6097/975/DC1
Materials and Methods
Figs. S1 to S18
Table S1
References (*30*–*44*)
PDB Coordinates of Lowest-Energy Glycosylated PFK1 Structure

22 March 2012; accepted 29 June 2012
10.1126/science.1222278

Neurexin and Neuroligin Mediate Retrograde Synaptic Inhibition in *C. elegans*

Zhitao Hu,[1,2] Sabrina Hom,[1,2,3] Tambudzai Kudze,[1] Xia-Jing Tong,[1,2] Seungwon Choi,[1,2,3] Gayane Aramuni,[4] Weiqi Zhang,[5] Joshua M. Kaplan[1,2,3]*

The synaptic adhesion molecules neurexin and neuroligin alter the development and function of synapses and are linked to autism in humans. Here, we found that *Caenorhabditis elegans* neurexin (NRX-1) and neuroligin (NLG-1) mediated a retrograde synaptic signal that inhibited neurotransmitter release at neuromuscular junctions. Retrograde signaling was induced in mutants lacking a muscle microRNA (miR-1) and was blocked in mutants lacking NLG-1 or NRX-1. Release was rapid and abbreviated when the retrograde signal was on, whereas release was slow and prolonged when retrograde signaling was blocked. The retrograde signal adjusted release kinetics by inhibiting exocytosis of synaptic vesicles (SVs) that are distal to the site of calcium entry. Inhibition of release was mediated by increased presynaptic levels of tomosyn, an inhibitor of SV fusion.

In *Caenorhabditis elegans*, a retrograde synaptic signal from muscle to motor neurons inhibits acetylcholine (ACh) release at neuromuscular junctions (NMJs) (*1*). This retrograde signal is induced by inactivation of a muscle microRNA (miR-1) and is abolished by inactivating the transcription factor MEF-2, a miR-1 target (*1*). In *mir-1* mutants, endogenous and evoked excitatory postsynaptic currents (EPSCs) recorded from body muscles were both diminished (Fig. 1), whereas synapse density is unaltered (*1*). Quantal content was significantly reduced in *mir-1* mutants, indicating decreased ACh release during evoked responses (Fig. 1E).

Because postsynaptic neuroligin promotes maturation of presynapses and stimulates neurotransmitter release in mice (*2*–*4*), we tested the idea that *C. elegans* neurexin (NRX-1) and neuroligin (NLG-1) are required for the retrograde signal. Consistent with this idea, the endogenous and evoked EPSC defects observed in *mir-1* mutants were eliminated in *mir-1*; *nlg-1* and *mir-1; nrx-1* double mutants (Fig. 1 and fig. S1). Retrograde inhibition of ACh release in *mir-1; nlg-1* double mutants was reinstated by transgenes expressing NLG-1 in cholinergic motor neurons but not by those expressed in body muscles. Analogous rescue experiments suggested that NRX-1 functioned in body muscles (fig. S1, B and D).

The *nlg-1* promoter expressed green fluorescent protein (GFP) in cholinergic motor neurons but not in GABAergic neurons (fig. S2, A and B). When expressed in cholinergic DA and DB motor neurons, NLG-1::GFP exhibited a punctate distribution in dorsal cord axons but was diffuse in ventral cord dendrites (fig. S2C). Dorsal cord NLG-1 puncta colocalized with a synaptic vesicle (SV) marker (mCherry-tagged UNC-57 endophilin) (fig. S2C) (*5*). NRX-1::GFP expressed in body muscles was also punctate in the nerve cords, and these NRX-1 puncta were often closely apposed to presynaptic UNC-57 puncta (fig. S2D). Thus, NLG-1 and NRX-1 were pre- and postsynaptic, respectively, at cholinergic NMJs, opposite in polarity to their mammalian counterparts. Other examples of reversed polarity include presynaptic NLG-1 in worms (*6*, *7*) and postsynaptic mouse and fly neurexins (*8*–*10*).

If trans-synaptic adhesion mediates the retrograde signal, NRX-1 should bind directly to NLG-1. In transfected cells, we expressed a truncated NRX-1 containing the putative neuroligin binding site (LNS6) (NRX-1[LNS6/HA]) and a soluble NLG-1 containing the entire extracellular domain fused to the immunoglobulin G Fc domain (NLG-1/Fc) (fig. S3). As expected, a significant fraction of NRX-1[LNS6/HA] bound to NLG-1/Fc when calcium was added but not when calcium was omitted (fig. S3B, lanes 4 and 5). No binding was observed between Fc and NRX-1[LNS6/HA] (lanes 2 and 3).

Next, we analyzed *nlg-1* and *nrx-1* mutants for altered synapse development. Cholinergic NMJs were visualized with GFP-tagged pre- (SNB-1 synaptobrevin) and postsynaptic (ACR-16 ACh receptors) markers (fig. S4). The fluorescent intensity and density of pre- and postsynaptic puncta were unaltered in *nlg-1* and *nrx-1* mutants. The rate and amplitude of endogenous EPSCs were also unchanged in *nlg-1* and *nrx-1* mutants (Fig. 1B and fig. S1B). Therefore, inactivation of NLG-1 and NRX-1 did not grossly alter the morphology or formation of cholinergic NMJs.

If NRX-1 mediates the retrograde signal, its expression or function should be altered in *mir-1* mutants. Consistent with this idea, the fluorescent intensity of postsynaptic NRX-1 puncta was increased in *mir-1* mutants (40% increase, $P < 0.001$), and this effect was eliminated in *mir-1 mef-2* double mutants (Fig. 1, F to H), in which retrograde signaling is abolished (*1*). Thus, inducing the retrograde signal increased postsynaptic NRX-1 levels, consistent with NRX-1 acting downstream of miR-1 in this pathway. The NRX-1::GFP construct contains a promoter (*myo-3*) and 3′ untranslated region (*unc-54*) that are not regulated by miR-1 (*1*); consequently, the effects of miR-1 and MEF-2 on NRX-1 expression are likely mediated by an indirect mechanism.

How does the retrograde signal alter ACh release? Evoked responses in *mir-1* mutants had decreased amplitude (Fig. 1E), faster decay (Fig. 2, A and B), and faster charge transfer (Fig. 2, C and D). To determine if these effects were caused by intrinsically faster muscle ACh responses, we analyzed endogenous EPSCs, which correspond to responses evoked by one SV fusion (*11*). Because endogenous EPSC kinetics were unaltered in *mir-1* mutants (fig. S5), the smaller evoked responses in *mir-1* mutants most likely resulted from faster and more abbreviated ACh release.

By contrast, quantal content was significantly increased when the retrograde signal was inactivated (in *nrx-1* and *nlg-1*mutants) (Fig. 1E and fig. S1D) but was not further increased in *nrx-1; nlg-1* double mutants (*nlg-1* $n = 13$, 872.1 ± 109.3; *nrx-1; nlg-1* $n = 6$, 712.7 ± 53, $P = 0.32$), consistent with NLG-1 and NRX-1 functioning together in this process. In *nlg-1* mutants, evoked responses exhibited slower decay and slower charge transfer, which were rescued by transgenes

[1]Department of Molecular Biology, Massachusetts General Hospital, Boston, MA 02114, USA. [2]Department of Neurobiology, Harvard Medical School, Boston, MA 02115, USA. [3]Program in Neuroscience, Harvard Medical School, Boston, MA 02115, USA. [4]Max Planck Institute of Neurobiology, D-82152 Martinsried, Germany. [5]Department of Psychiatry, University of Münster, D-48149 Münster, Germany.

*To whom correspondence should be addressed. E-mail: kaplan@molbio.mgh.harvard.edu